Experimental investigation of the effects of aggregate size distribution on the fracture behaviour of high strength concrete

1. A. P. N. Siregar

Civil Engineering Department, Tadulako University, Indonesia.

Email : a.siregar@surrey.ac.uk

2. M. Imran Rafiq (corresponding author)

School of Environment and Technology, University of Brighton, United Kingdom.

Email : m.rafiq@brighton.ac.uk
Tel: : +44-1273-642163

3. M. Mulheron

Department of Civil and Environmental Engineering, University of Surrey, United Kingdom.

Email : m.mulheron@surrey.ac.uk

Abstract: This paper examines the influence of different aggregate size distributions on the fracture behaviour of high strength concrete. Three-point bend test was performed on 63 notched beams casted using three aggregate size distributions and two water to binder ratios. The total fracture energy, G_F, and critical stress intensity factor, K_{IC}, were used to determine the fracture characteristic of concrete. The results show that the values of G_F decrease substantially with increasing coarseness of aggregate grain structure, λ. Values of K_{IC} also decreased but demonstrated only limited dependence on λ. In contrast, reducing the total w/b ratio substantially increases the value of K_{IC} but had no measurable effect on G_F.

Keywords *Aggregate size distribution, Aggregate grading, Fracture energy, Stress intensity factors, size effect;*

Highlights:

- Aggregate size distribution affects the fracture behavior of high strength concrete
- Fracture energy and stress intensity factors measured for 63 notched beams

- Strong dependence of fracture energy upon aggregate size distribution.
- Limited dependence of stress intensity factor upon aggregate size distribution.
- Reducing the water to binder ratio increases the stress intensity factor
- Reducing the water to binder ratio have no measurable effect on the fracture energy.
- Maximum value of fracture energy for high strength concrete is limited by the strength of aggregates used.

1 Introduction

Concrete is widely used in the construction of buildings, bridges and other infrastructure around the world. Its use is driven by its flexibility of form, the relative simplicity of manufacture and the widespread availability of both binder materials, such as Portland cement, and inert, graded, granular aggregates. As a particulate composite material, the physical and mechanical properties of hardened concrete are strongly influenced by both its constituent materials and the proportions in which they are combined. The aggregate typically occupies more than 70% of the volume of a concrete mix and plays an important role in determining the physical properties and mechanical behaviour of both the fresh and hardened material (Chen and Liu 2004). The interactions that occur at the interface between the aggregate particles and the cement paste which surrounds and binds them influences many of the properties of hardened concrete, including strength, stiffness and fracture toughness. Historically, normal strength concrete, with a compressive strength of less than 50 MPa, has been used in the construction of plain, reinforced and prestressed concrete structures (Comitte Euro-International du Beton 2010). However, over the past 30 years, there has been increasing use of, and reliance on, so-called high-strength concrete for the creation of ultra-high-rise buildings and long-span bridges (Wolinski et al. 1987;

American Concrete Institute 2010). High-strength concretes routinely have compressive strengths in the range 60-90 MPa although much higher values can be achieved. This requires good mix design, the appropriate selection of constituent materials combined with the use of specialised admixtures. As a consequence, there is significant interest in understanding the mechanisms that govern the failure behaviour of such high-strength ceramic composites.

Whilst the fracture resistance of Portland cement concrete is known to be dependent on its compressive strength and water/binder ratio, w/b, other parameters such as the size, shape, surface texture, and volume fraction of the aggregate have also been found to influence the fracture mechanics parameters of hardened concrete (Hillerborg 1985; Wolinski et al. 1987; Mihashi et al. 1991; Zhou et al. 1995; Wu et al. 2001; Xiao et al. 2004; Elices and Rocco 2008; Ince and Alyamac 2008; Königsberger et al. 2014). In normal strength concrete both the fracture toughness, i.e. the critical stress intensity factor, K_{IC}, and the fracture energy, G_F, of concrete have been found to increase with the compressive strength of the concrete (Ince and Alyamac 2008), and the maximum aggregate size (Hillerborg 1985; Wolinski 1987; Mihashi 1991) and volume fraction of the aggregate (Amparano and Roh 2000). Similar behavior have also been reported for the self compacted concrete (Karamloo et al. 2016). However, aggregate type, and associated particle shape and surface texture has been found to have little effect on the facture energy of normal strength concrete (Wu et al. 2001; Xiao et al. 2004).

The compressive strength of high strength concrete also affects the measured values of both K_{IC} and G_F (Wu et al. 2001; Xiao et al. 2004), which increases as

the maximum aggregate size increases (Chen and Liu 2004). Unlike normal strength concrete, the values of G_F for high-strength concrete have been found to be sensitive to the aggregate type (Zhou et al. 1995; Xiao et al. 2004). Other results for high–strength concrete show that K_{IC} increases as the w/b ratio decreases (Ince and Alyamac 2008). Thus, the w/b ratio and properties of the aggregate both control the compressive strength and influence the fracture behaviour of high-strength concrete. Hence, for simplicity, compressive strength is widely used as an input parameter for calculating G_F along with the maximum aggregate diameter (Committee Euro-International du Beton 1993; Bazant and Becq-Giraudon 2002). However, the results of Chen and Liu (2004), and Ackay et al. (2012), indicate that both K_{IC} and G_F of normal and high-strength concretes are influenced by the volume fraction of coarse aggregate. This is because the dissipated fracture energy is dependent on the physical characteristics of the crack path through the concrete. A tortuous crack path, with associated micro-cracking, crack-bridging and aggregate interlocking will result in the absorption of more energy than a smooth crack path. The path of a crack during fracture will be influenced by the coarseness of internal random grain structure of the concrete, λ, which is itself dictated by aggregate grading (Amparano and Roh 2000). This suggests that aggregate grading can influence the fracture behaviour of concrete.

In high-strength concrete, the propagation of cracks, whether passing round or through the aggregates, is dominated by the quality and distribution of the various size of aggregates (Issa et al. 2003). When using high-quality aggregates, the aggregate grading (and associated particle-size distribution) is a significant factor in controlling the coarseness of the internal random grain structure of concrete and influences the crack path that develops during the fracture process. Chen and Liu

(2004), and Ackay et al. (2012) have noted that whilst the volume fraction of coarse aggregate is thought to influence both K_{IC} and G_F of concrete there remains a lack of experimental evidence in this area. Since the volume fraction of coarse aggregate reflects the aggregate size distribution, understanding the fracture behaviour of concrete based on its aggregate size distribution is important. Therefore, the objectives of this study were to investigate the role of aggregate size distribution and w/b ratio on the fracture behaviour of high-strength concrete and resulting values of K_{IC} and G_F.

2 Experimental setup

2.1 Materials

Flinty river gravel from the Thames Valley river was used for coarse aggregate with sizes in the range of 5 mm to 16 mm. The fine aggregate was a natural river gravel of size ranging from 4 mm down to 0.30 mm. A CEM Type I with a specific surface area of 338 m^2/kg was employed in the mix combining additional Pulverized Fuel Ash (Fly Ash) conforming to BS EN450-S category B. A slurry-based silica fume was also involved in some of the concrete mixes. A super-plasticiser was employed to allow appropriate workability of the fresh concrete.

The concrete mix proportions of each material used are shown in Table 1. A total of six different concrete mixes were produced employing three aggregate grading curves, designated as ‘A’, ‘B’ and ‘C’, see Figure 1. To achieve the appropriate grading a batch of the as-received aggregate was sieved into its component fractions and the required amount of each fraction was then recombined. Two total water to binder (w/b) ratios of 0.20 (equivalent to a free w/b ratio of 0.17 ±

0.02) and 0.30 (equivalent to a free water/binder ratio of 0.23 ± 0.01) were used, and were designated as '1' and '2' respectively, see Table 1. Thus, mix 'A1'indicates a mix with aggregate grading type 'A' and a total w/b ratio of 0.20.

Table 1 Mix proportions of the six concrete mixes tested.

Mix	w/b*	Unit weight (kg/m^3)						
		Aggregate		Cement	PFA	Silica fume	Water	Super-plasticiser
		Coarse	Fine					
A1	0.20	1108	499	547.7	76.7	54.7	135.9	2.64
A2	0.30	1108	499	679	-	-	203.7	1.61
B1	0.20	1552	54	547.7	76.7	54.7	135.9	2.01
B2	0.30	1552	54	679	-	-	203.7	1.42
C1	0.20	1322	284	547.7	76.7	54.7	135.9	2.27
C2	0.30	1322	284	679	-	-	203.7	1.50

*Total water/binder ratio

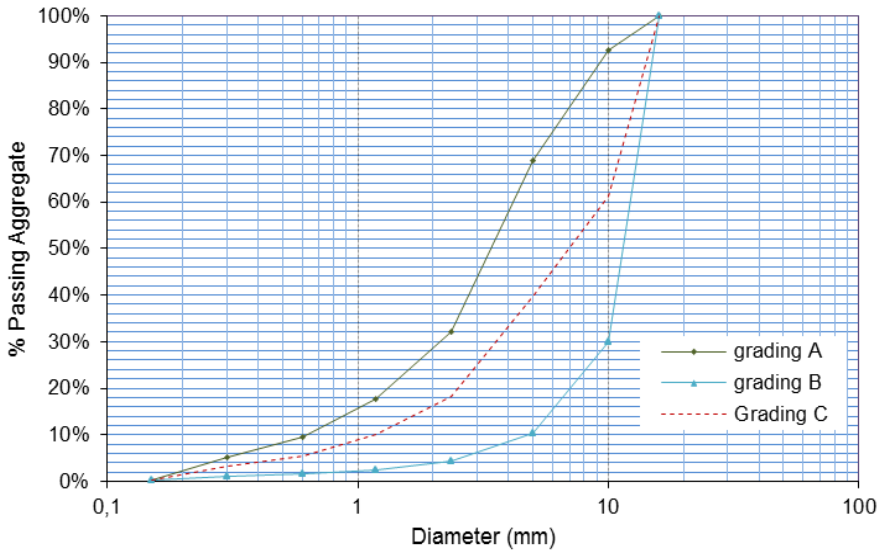

Fig.1 Aggregate grading curves for types 'A', 'B', and 'C'.

It is well established that the workability of fresh concrete, as measured by its consistence, has a profound effect on the ease of compaction of the material and that incomplete compaction can adversely affect the properties of the resulting hardened concrete (Neville and Brook 1990). As a consequence, the consistence of all the mixes used in this study was kept constant, the target slump value for all the mixes was 120 ± 20 mm (equivalent to a consistence class S3 as prescribed by

ENV 206, Part 1: 2000). This was achieved by varying the quantity of super-plasticiser in each mix, Table 1. Since the aggregate to binder ratio is also known to affect the concrete properties, it is kept constant for all mixes used in this study.

2.2 Specimens and Test Setup

At least nine 100 x 100 x 100 mm cubes were tested to determine the average compressive strength of the hardened concrete, following BS EN 12390: Part 3(2000). The fracture behaviour of the hardened concrete was determined using 100 x 100 x 850 mm beam specimens tested in three-point bend (TPB) following RILEM TC 50-FCM (1985). All of the specimens were de-moulded approximately 24 hours after casting and cured under water at 22 ± 2 °C for 30 days prior to testing.

Figure 2 shows the dimension of the notched beam specimen for the associated three-point bend test arrangement. The depth (d), the width (t) and the total length (L) of the beam was 100, 100, and 850 mm respectively with a support span (S) of 800 mm. A notch depth (a_o) of 25 mm and width of 2.5 mm was created in all of the specimens prior to testing.

The TPB test was carried out using a closed-loop servo-hydraulic testing machine with a maximum load capacity of 600 kN. The applied load was measured using a 10 kN load cell. The loading rate was controlled by applying a vertical displacement of 0.01 mm/s, following the methodology developed by Zhang at al. (2009). A calibrated linear variable differential transducer (LVDT) was employed to measure the vertical deflection of the beam at the loading point. A clip gauge was used to quantify the crack mouth-opening displacement, Figure 2.

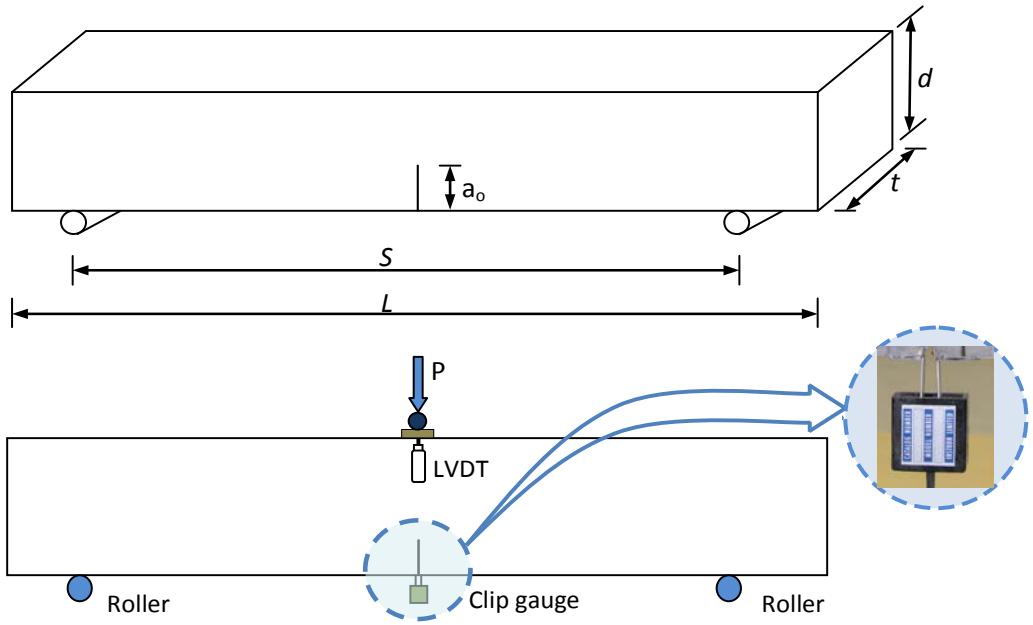

Fig. 2 Geometry of specimen and test set up showing detail of clip gauge attachment

3 Concrete properties

The measured values of slump of the fresh concrete and the compressive strength of the hardened concrete, tested at 30 days, are presented in Table 2. It can be seen that the average slump of all the mixes were controlled within the target range 120 ± 20 mm.

The average compressive strength of the concrete mixes with a total w/b ratio of 0.30 (equivalent to a free water/binder ratio of 0.23 ± 0.01) ranged from 66-68 MPa. The average compressive strength of the concrete mixes with a total w/b ratio of 0.20 (equivalent to a free w/b ratio of 0.17 ± 0.02) ranged from 85-98 MPa. These results are in agreement with the well-known Abrams' law (Mindess and Young 1983) in that the measured compressive strength increases with decreasing w/b ratio. Whilst the w/b ratio is the main factor dictating the

compressive strength of hardened concrete, local changes in the size, shape and distribution of the aggregates within individual test specimens contributes to the measured variability. However, this variability is within normal limits for high strength concrete mixes.

Table 2 Slump, mean (30-day) compressive strength and coarseness ratio of concrete mixes

Mix	Slump			Compressive strength			λ
	mm	N	S	MPa	N	S	
A1	110	4	4.4	85.2	12	5.7	0.32
B1	100	4	6.4	97.6	12	1.4	0.22
C1	115	3	6.3	94.8	9	2.6	0.25
A2	100	4	6.8	68.2	12	3.6	0.32
B2	120	3	5.5	66.0	9	2.9	0.22
C2	130	3	7.8	68.4	9	0.8	0.25

N= number of test specimens, S= Standard deviation of sample, λ = coarseness of internal random grain structure.

4 Coarseness of internal random grain structure (λ), and fracture characteristic (K_{IC} and G_F) of concrete

The coarseness of the internal random grain structure of the hardened concrete, λ, is presented in Table 2, and the derived fracture characteristics of the concrete, i.e. K_{IC} and G_F, are presented in Table 3 and these are considered in more detail in the following sub-sections.

4.1. Coarseness of internal random grain structure of concrete

According to Amparano and Roh (2000) the coarseness of the internal random grain structure of concrete, λ, is defined as:

$$\lambda = \frac{1}{D_{ave}(1-V_a)} \quad \text{Eq. (1)}$$

where, D_{ave}, is the average diameter of the aggregate particles, and V_a is the volume fraction of the coarse aggregate (above 4 mm) calculated from the mix design parameters of this study (Table 1) and the grading curves shown in Figure 1. It can be seen from Eq. (1) that the value of λ is dependent on both the volume fraction and average diameter of coarse aggregate and is considered to be an important factor affecting the dissipated fracture energy in concrete. The effect of the aggregate grading used in the concrete mix tested in this study produced different values of λ, i.e. 'B' - low (λ = 0.22), 'C' - medium (λ = 0.25) and, 'A' - high (λ = 0.32), see Table 2.

4.2 Fracture energy

One parameter that has been widely used to characterise the fracture behaviour of brittle composite materials such as concrete is the fracture energy, G_F. In this study, values of G_F (for each specimen) were calculated from the corresponding load vs mid-span deflection curve, Figures 3(a) and 3(c). By following the recommendations of RILEM TC50-FCM (RILEM 1985) it was possible to account for the effects of the self-weight of the beam:

$$G_F = \frac{W_o + mg\delta_o}{(d-a_o)t} \quad \text{Eq (2)}$$

where, G_F is the total fracture energy, W_o is the area under the load-deflection curve, m is the total mass of specimen between supports, g is the gravitational constant, δ_o is the deflection at failure, d is the height of the sample, a_o is the depth of the notch and t is the width of the sample. Values of the mean fracture energy and standard deviation for the samples tested are presented in Table 3.

The fracture energy dissipated during the failure process of concrete can be related to the crack opening, which drives the crack forward. This was monitored by the load vs crack mouth-opening displacement (CMOD) curves, Figures 3(b) and 3(d). These were used to assist analysis of the crack-opening behaviour in the post- peak stress regime.

4.3 Critical stress intensity factor (K_{IC})

In considering the tensile fracture of concrete it is important to consider the role of inherent defects, such as cracks, in limiting the stress that can be supported by a given section of material. In the case of brittle ceramic materials, such as concrete, the role of cracks can be successfully modeled on the basis of linear elastic fracture mechanic-LEFM (Shah and Ahmad 1994). This approach assumes that a suitably oriented crack within the material will start to propagate when the (mode I) stress intensity factor K_I , at the crack tip exceeds the critical stress intensity factor, K_{IC}, which is also know as the fracture toughness (Zhang and Xu 2011). At its simplest K_I can be considered to be a measure of the force tending to cause fast fracture whilst K_{IC} is a material property, like stiffness and Poisson's ratio that is a measure of the materials resistance to crack growth. In a brittle material containing a crack (of given size) and subject to an externally applied stress fast

fracture will not occur provided that $K_I < K_{IC}$. Determination of the appropriate stress intensity factor is complicated by the fact that K_I is a function of the crack length, the local (and global) geometry, the value and mode of the externally applied load and associated boundary conditions (Shah et al. 1995).

In this study the LEFM approach has been used to analyse the effect of the three different aggregate size distributions on the fracture characteristic of high-strength concrete tested in three-point bend up to the peak stress. The values of K_{IC} for the individual test samples was carried out following the RILEM TC89-FMT (RILEM 1990):

$$K_{IC} = \frac{3(P_c+0.5W)\left[S(\pi a_c)^{0.5} g\left(\frac{a_c}{d}\right)\right]}{2d^2 t} \quad \text{Eq. (3)}$$

in which,

$$g\left(\frac{a_c}{d}\right) = \frac{1.99-\left(\frac{a_c}{d}\right)\left(1-\frac{a_c}{d}\right)\left[2.15-3.93\left(\frac{a_c}{d}\right)+2.70\left(\frac{a_c}{d}\right)^2\right]}{\sqrt{\pi}\left[1+2\left(\frac{a_c}{d}\right)\right]\left[1-\left(\frac{a_c}{d}\right)\right]^{\frac{3}{2}}} \quad \text{Eq. (4)}$$

where, P_c is the critical maximum load, W is the beam's self-weight, S is span of specimen, a_c is the critical effective elastic crack length, d is the specimen depth, and t is the specimen width. The mean, and standard deviation, of the calculated values of K_{IC} are presented in Table 3.

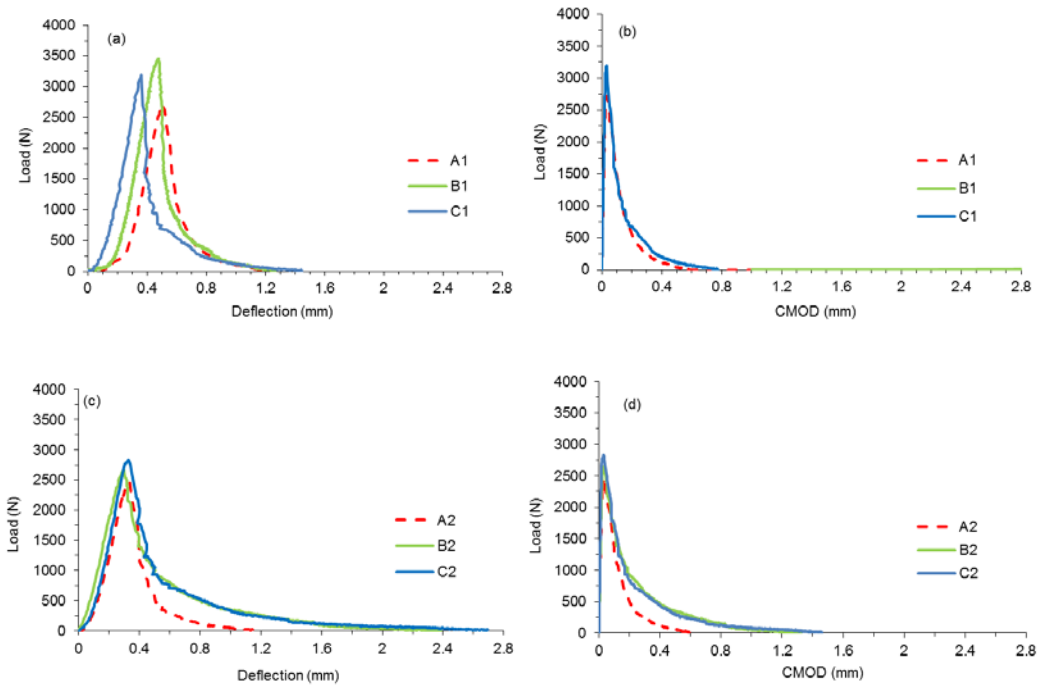

Fig. 3 Typical load-deflection and associated load-CMOD curves for concrete with; w/b = 0.2 (3(a) & 3(b), and w/b = 0.30 (3(c) & 3(d).

Table 3 Fracture energy and critical stress intensity factor for concrete mixes.

Mix	w/b ratio	Number of samples	Mean G_F	S	Mean K_{IC}	S
			N/m	N/m	MPa.m$^{1/2}$	MPa.m$^{1/2}$
A1	0.2	12	93.8	9.1	0.99	0.07
B1	0.2	12	149.9	10.6	1.24	0.11
C1	0.2	9	126.7	14.1	1.26	0.12
A2	0.3	12	85.1	10.4	0.78	0.05
B2	0.3	9	146.5	13.3	0.93	0.11
C2	0.3	9	134.3	11.2	0.71	0.09

S= Standard deviation of sample

5 Discussion

5.1 Effect of aggregate size distribution

According to Hillerborg and Modeer (1976) the pre-peak tensile response of concrete can best be assessed by examining the stress-strain relationship of the material whilst the post-peak fracture behaviour, or "softening term", can be most accurately assessed by investigating the stress-crack opening curve. In this study both approaches have been employed to help further elucidate the role of aggregate size distribution on the fracture behaviour of both normal and high-strength concrete.

The values of G_F are dependent on the shape and form of the softening curve making comparisons between samples of the same material and between batches of different materials complicated. As a consequence, normalised stress (Stress/Peak Stress) vs deflection curves were used in the analysis of the post-peak fracture behaviour of the concrete mixes tested. Figure 4(a) compares the typical deflection and CMOD response obtained for the high-strength concrete mixes A1, B1 and C1 (w/b ratio = 0.2).

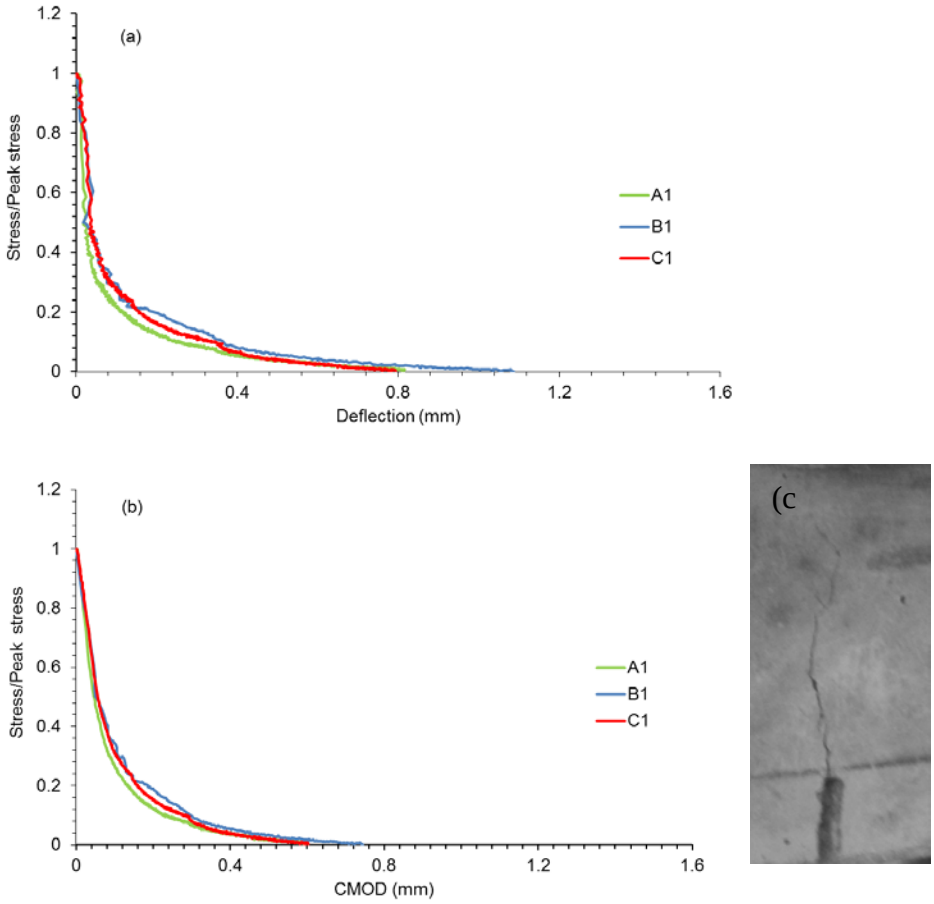

Fig. 4 Softening response of three point bending test of concrete with w/b ratio of 0.20 (a) post-peak stress-deflection curve (b) post-peak stress-CMOD curve (c) crack path of specimen

It can be seen that there is little difference in the curves obtained for the three aggregate gradings suggesting that similar processes are at play although the contribution to the total energy absorbed may be different. Indeed it is interesting to compare the fracture energy obtained for mixes B1, C1 and A1 (ranked in terms of their grain size distribution), which yields the values of G_F of 149.9, 126.7 and 93.8 N/m for λ's of 0.22, 0.25 and 0.32 respectively, see Tables 2 & 3 and Figure 6(b). Hence for the high-strength concrete, reduction of coarser aggregate sizes in the mix (represented by an increase in λ *value)* is associated with a significant reduction in the measured fracture energy. This result is in line

with, and confirms, previously published results (Chen and Liu 2004). The values of G_F obtained for these mixes may be compared with the measured values of K_{IC} of 1.24 (B1), 1.26 (C1) , and 0.99 (A1) MPa.m^{½} respectively for the same samples, Table 3. This suggests that the critical stress intensity factor to initiate crack growth is relatively insensitive to the internal random grain structure of concrete, albeit slightly higher for higher proportions of coarse aggregates in the mix, Figure 6(a).

The above results may be compared with those for mixes A2, B2 and C2, Figure 5(a). For these concretes, which have a w/b ratio of 0.3, the normalised curves obtained demonstrate both a greater variation with the change in λ and a somewhat slower rate of decay of normalised stress per unit deflection than seen in Figure 4(a). This suggests that the aggregate size distribution is influencing the post-peak fracture behaviour in a different way to that of the higher strength mixes. Again it is interesting to compare the fracture energy obtained for these mixes when ranked in terms of the grain size distribution, i.e. B2, C2 and A2, which yields values of G_F of 146.5, 134.3 and 85.1 N/m respectively. These values of G_F, which are in close agreement with those for mixes A1, B1, and C1 (see Table 3), confirm the observation that reducing the coarser grain size in the mix (increasing λ) is associated with lower fracture energy. That is to say the degree of coarseness of internal random grain structure plays a role in the energy absorption process during the fracture of hardened concrete. As with the higher strength mixes measured values of K_{IC} are, when compared to G_F, relatively insensitive to changes in λ, see Figure 6(a). The influence of w/b ratio on both G_F and K_{IC} is discussed in section 5.2.

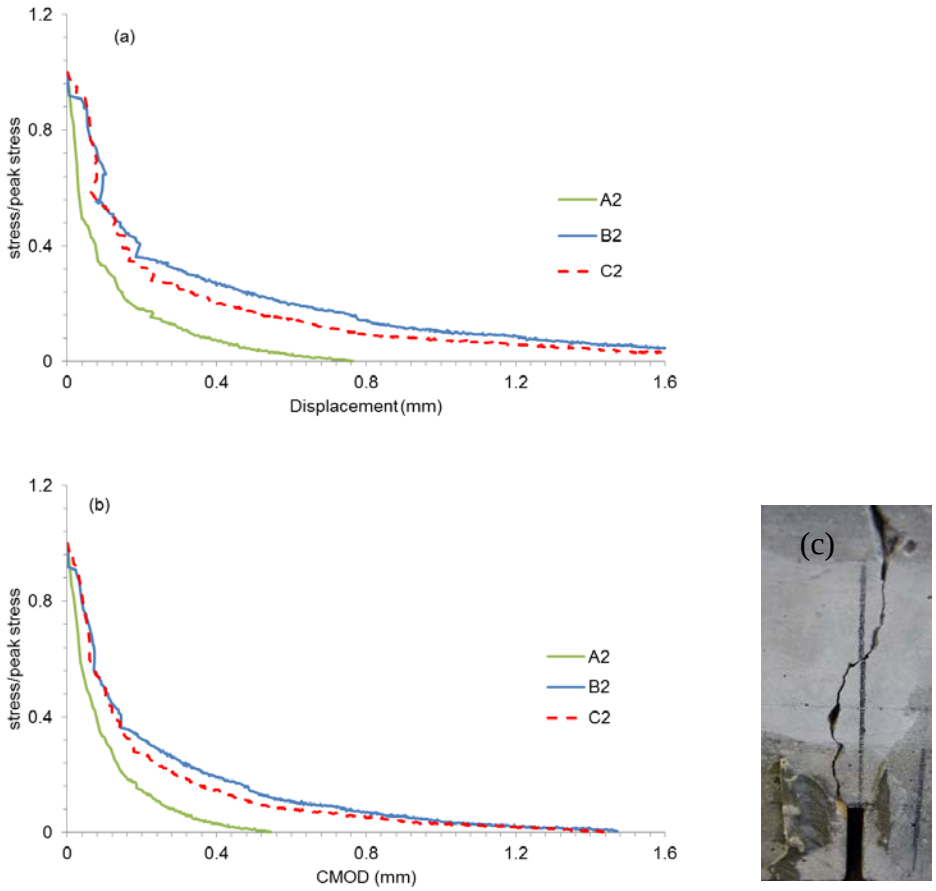

Fig. 5 Softening response of three point bending test of concrete with w/b ratio of 0.30 (a) post-peak stress-deflection curve (b) post-peak stress-CMOD curve (c) crack path of specimen

Having established the impact of λ on both G_F and K_{IC} it is useful to consider factors which may be contribute to the overall fracture process. The interfacial zone properties and aggregate properties such as size distribution and surface texture can play an important role in resisting crack opening. Since the aggregate used in these experiments was from a single source, it has been assumed that the effect of aggregate surface texture can be safely ignored. Altering the w/b ratio has the potential to change the stiffness (and strength) of the interfacial zone that exists between the aggregate and the cement matrix. If the strength of the

363 aggregate particles is more than that of the interfacial zone matrix, the aggregate
364 particles can act as crack growth arresters in the fracture process (Giaccio and
365 Zerbino 1998). Other toughening mechanisms such as micro-crack shielding and
366 particle bridging can also assist in the increase of the fracture resistance of
367 concrete when the aggregate has not failed, i.e. the crack propagates only within
368 the interfacial zone or through the cement paste. For such a case, the crack path
369 would be expected to show a strong correlation with λ, i.e. higher coarseness of
370 internal grain structure of concrete would lead to a more tortuous crack path and
371 vice versa. This mechanism could explain the longer "tail" in the post-peak stress
372 vs displacement curve of Figures 5(a) which was obtained with the lower strength
373 concrete (i.e. higher w/b ratio). In contrast, if the strength of the aggregate is less
374 than that of the interfacial zone matrix, the crack becomes able to propagate
375 through the aggregate particles, and is thus less sensitive to λ. Such behaviour
376 would be expected to produce a relatively straight crack path (Figure 4 (c)) and
377 smaller "tail" in the post-peak curve such as the one shown in Figure 4(a) for the
378 higher strength concrete tested here. Hence, the fracture characteristic of high
379 strength concrete can be assessed on the basis of the fracture parameters and the
380 slope of the post-peak curves.
381
382 It should be remembered that a crack will only propagate if the stress intensity at
383 the crack tip is greater than K_{IC}. The propagation of a growing crack during a
384 three-point bend test is related to the crack opening, which can be analysed
385 through normalised stress versus CMOD curves, Figures 4(b) and 5(b). Although
386 this is a qualitative analysis, it suggests that whilst internal random grain structure
387 influences the crack opening in the high w/b ratio concrete (Fig. 5b), its affect at

388 low w/b ratios is small (Fig. 4b). This suggests that the influence of grain size
389 distribution on the crack opening decreases with concrete strength, see section 5.2.
390

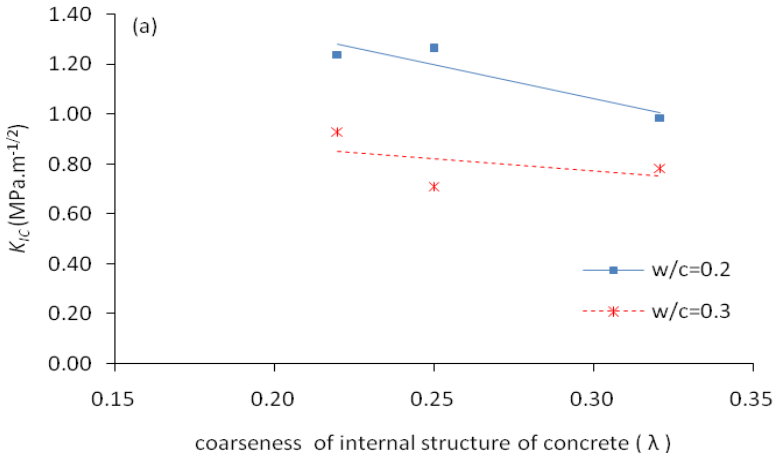

391

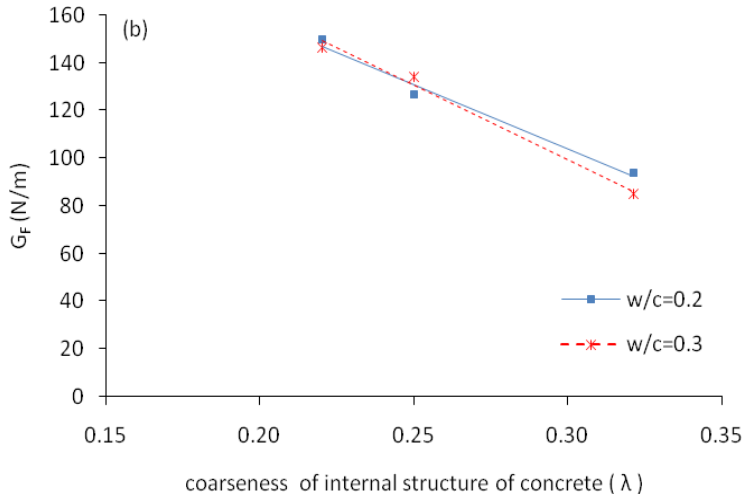

392

393 **Fig. 6** The effect of coarseness of internal structure of concrete on (a) the stress
394 intensity factor (K_{IC}) and, (b) fracture energy (G_F)

395 It can also been seen from Figure 4 and 5 that the level of ductility varies
396 considerably for the beams with different aggregate size distribution and w/b ratios.
397 Ductility ratio for the beams is computed to analyze this further and is shown in Table
398 4. Ductility ratio is taken as the ratio of the deflection of beam at failure to deflection
399 of beam at the yield point (Rao et al., 2010). The Table clearly demonstrates that the

aggregate size distribution and w/b ratio significantly influences the level of ductility exhibited by high strength concrete.

	Gradation of aggregate					
	A1	B1	C1	A2	B2	C2
yield deflection (mm)	0.5	0.41	0.39	0.33	0.28	0.33
max deflection (mm)	1.20	1.47	1.42	1.17	2.34	2.68
Ductility ratio of beam	**2.4**	**3.6**	**3.6**	**3.6**	**8.4**	**8.1**

5. 2 Effect of water/binder ratio

Figure 7 shows the effect of w/b on the measured compressive strength, f_c, critical stress intensity factor, K_{IC}, and fracture energy, G_F of the six concrete mixes tested.

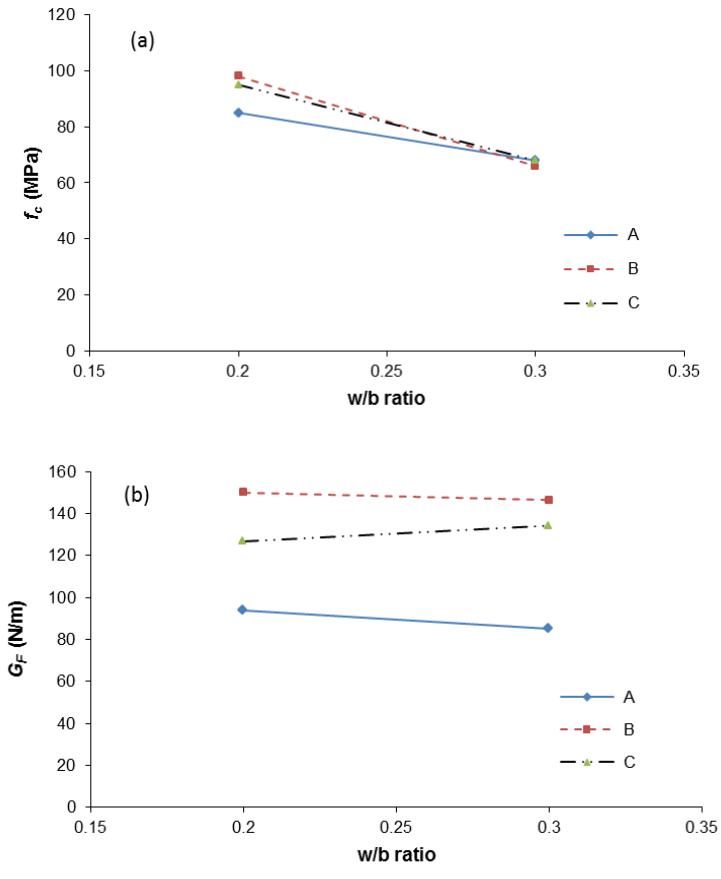

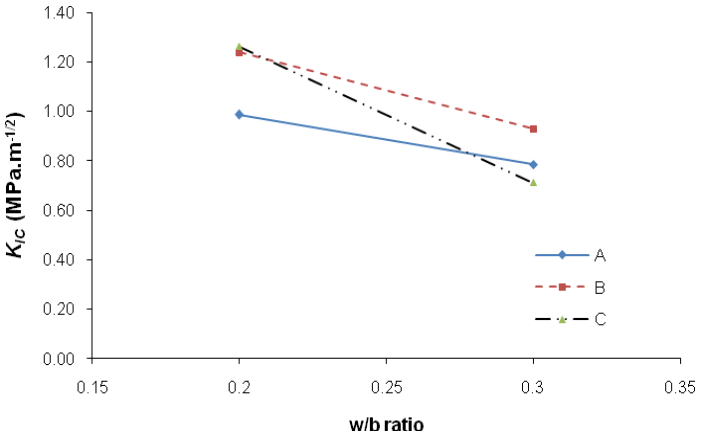

409

410 **Fig. 7** The effect of w/b ratio on (a) compressive strength, (b) fracture energy,

411 and(c) critical stress intensity factors

412

413 As might be expected f_c was found to decrease as the w/b ratio increased, Figure

414 7(a). Similarly K_{IC} sensibly decreased with increasing w/b ratio, Figure7(c). In

415 contrast G_F was found to be insensitive to w/b ratio, Figure 7(b). This behaviour

416 reflects the result of the hydration process (Neville and Brook 1990) in that the

417 porosity level in the cement paste is related to the amount water in the mix which,

418 in turn, dictates the bond strength between the aggregate and the cement paste.

419 Moreover, supplementary cementitious materials, such as the PFA incorporated in

420 the high strength mixes used here, contribute by reacting with free calcium

421 hydroxide in the cement paste and induces in improvement in the matrix strength

422 (Köksal and Altun 2008). At the same time unhydrated particles of supplementary

423 cementitious materials will, by filling void space in the bulk paste, reduce the

424 porosity of paste and help the formation of a denser aggregate/cement interfacial

425 zone. Where the stiffness of interfacial zone and aggregate are similar, then

426 aggregate grading, which influences the bonding surface area and density of

427 concrete, can play an important role in distributing stress in the material and hence

428 influence the initiation of cracks. Therefore, w/b ratio and aggregate grading are

factors influencing the quality of the interfacial zone. Consequently, the reduction of w/b ratio of concrete from 0.30 to 0.20 increases K_{IC} by ≈ 26% and fc by a similar amount, ≈ 23%. At the same time, the measured values of G_F were found to essentially independent of w/b within the accuracy of the measurements. This is thought to be because, as elaborated in Section 5.1, the aggregate grading affects the dissipated fracture energy of concrete. Thus, G_F is dependent on the crack path and is influenced primarily by the quality of aggregate, which was kept constant, and the aggregate size distribution, which was varied.

The relationship between the measured fracture energy, G_F, and f_c, for compressive strength more than 60 MPa is shown in Figure 8, along with published data taken from Bazant and Becq-Giraudon (2002) for normal strength concrete (f_c < 50 MPa) with the same value of λ (= 0.25).

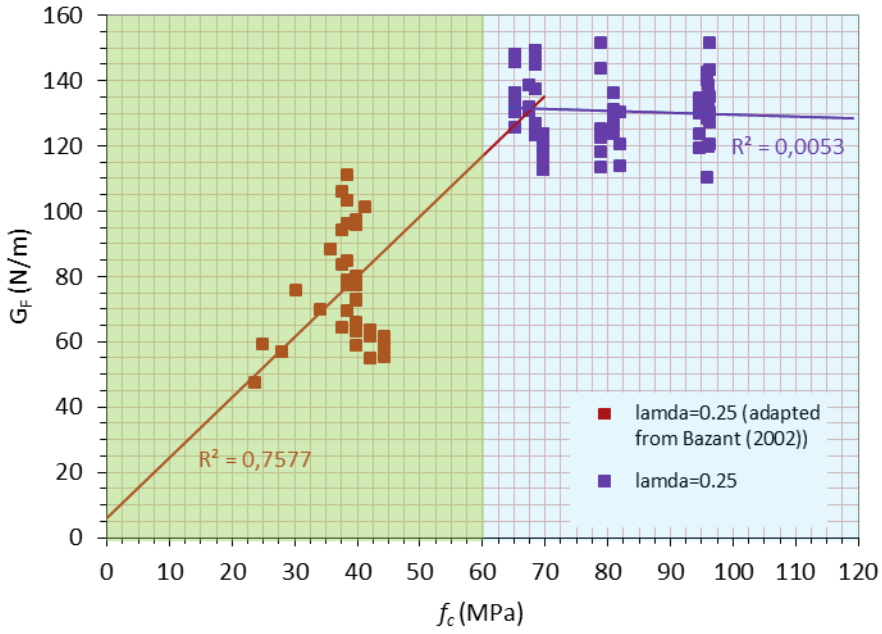

Fig. 8 Effect of compressive strength on the G_F of concrete

Although the experimental data shows some scatter, it can be seen that initially G_F increases linearly, and a regression on the trend line yields an f_c, $R^2 = 0.758$. This relationship holds where the concrete strength is below ≈ 60-70 MPa. However, where the strength of the concrete is above this value, G_F, remains at around 130 (± 20) N/m and appears unaffected by any increase in f_c, indeed a regression on the trend line yields an $R^2 = 0.005$ which suggests that the two variables are not correlated. Given that these results are for concrete manufactured with the same value of λ, this behaviour is not related to any change in the coarseness of internal random grain structure. Thus, for the normal strength concrete mixes ($f_c < 60 \pm 5$ MPa), where the fracture path is dominated by aggregate cement de-bonding (a more tortuous crack path exists), G_F increases with f_c (and hence w/b ratio) due to the improved strength of both the aggregate/cement bond and the cement matrix itself. When f_c exceeds ≈ 60 ± 5 MPa then the aggregate/cement bond strength is sufficient that the fracture path can pass through the aggregate particles. When this transition occurs the fracture path becomes dominated by aggregate failure and as a consequence G_F is limited by the strength of the aggregate despite the compressive strength of the concrete, f_c, continuing to increase. Therefore, the maximum value of G_F for a given high strength concrete will be limited by the strength of the aggregate.

6 Conclusions

The aim of this paper was to investigate the effect of aggregate size distribution (induced by aggregate grading) on the fracture behaviour of high-strength concrete. Based on a qualitative analysis of the post-peak softening curve

behaviour and a quantitative analysis of the measured fracture energy (G_F) and critical stress intensity factor (K_{IC}) the following conclusion can be drawn:

1. The compressive strength and critical stress intensity factor of the high-strength concrete demonstrated the expected dependence on the w/b ratio, i.e. increase in w/b ratio reduces both the compressive strength and the critical stress intensity factor.
2. The size distribution of the aggregate, measured using the coarseness of internal random grain structure of the concrete, λ, has a significant influence on the fracture energy of high strength concrete. Changing λ from 0.32 to 0.22 resulted in a 50% increase in measured values of G_F.
3. The critical stress intensity factor, K_{IC}, is relatively insensitive to the aggregate size distribution; however, higher proportion of coarser grain size tends to increase the $K_{IC.}$
4. On the basis of the measured values of G_F and the K_{IC}, the aggregate size distribution and w/b ratio were found to influence the level of ductility exhibited by high strength concrete.
5. The maximum value of G_F for a high strength concrete will be limited by the strength of the aggregate.

The fracture parameters obtained in these experiments enrich the factors which influence the fracture behaviour of high-strength concrete and can be used to further refine predicted fracture energy formula used in developing design criteria.

Acknowledgements The authors would like to acknowledge The Higher Education Directorate General, Ministry of National Education, Republic of Indonesia for the financial support for this project, and the University of Surrey for infrastructures, facilities and laboratories.

References

Ackay, B, Agar-Ozbek A. S., Bayramov, F., Atahan, H.N., Sengul, C., Tasdemir, M.A. (2012) Interpretation of aggregate volume fraction effects on fracture behaviour of concrete. Construction and Building Materials 28: 437-443.

Amparano F. E., Xi, Y., Roh Y. S. (2000) Experimental study on the effect of aggregate content on fracture behaviour of concrete. Engineering Fracture Mechanics 67: 65-84.

American Concrete Institute (2010) Report on high strength concrete. ACI-363R-10. Farmington Hills, USA.

Bazant Z. P. and Becq-Giraudon E. (2002) Statistical prediction of fracture parameters of concrete and implications for choice of testing standard. Cement and Concrete Research 32: 529-556.

Chen B. and Liu J. (2004) Effect of aggregate on the fracture behaviour of high strength concrete. Construction and building materials 18: 585-590.

Committee Euro-International du Beton (1993) CEB-FIP Model Code 1990. Thomas Telford, UK.

CommitteeEuro-International du Beton (2010) CEB-FIP Model Code 2010 (first draft). fib Bulletin 55: Model Code 2010, First complete draft – Volume 1, Lausanne, Switzerland.

Elices M. and Rocco C. G. (2008) Effect of aggregate size on the fracture and mechanical properties of a simple concrete. Engineering Fracture Mechanics 75(13): 3839-3851.

Giaccio G. and Zerbino R (1998) Failure mechanism of concrete: combined effect of coarse aggregate and strength level. Advance Cement Based Materials 7(2): 41-48.

Hillerborg A. A. (1985) Result of three comparative test series for determining the fracture energy G_F of concrete. RILEM materiaux et Constructions 18(107): 33-39.

Hillerborg A. A. and Modeer M. (1976) Analysis of crack formation and crack growth by means of fracture mechanics and finite element. Cement and Concrete Research(6): 773-782.

Ince, R. and Alyamac K. E. (2008) Determination of fracture parameters of concrete based on the water-cement ratio. Indian Journal of Engineering & Materials Sciences 15: 14-22.

Issa M. A., Issa M. A. Islam, Md.S., and Chudnovsky, A. (2003) Fractal dimension-a measure of fracture toughness and toughness of concrete. Engineering Fracture Mechanics 70(1): 125-137.

Karamloo, M., Mazloom, M., Payganeh, G. (2016) Effects of maximum aggregate size on fracture behaviour of self-compacting light weight concrete. Construction and Building Materials, 123, 508-515.

Köksal F. F. and Altun F. (2008) Combined effect of silica fume and steel fiber on the mechanical properties of high strength concretes. Construction and Building Materials 78(10): 1875-1880.

Königsberger M., Pichler B., and Hellmich, C. (2014) Micromechanics of ITZ-aggregate interaction in concrete Part II: Strength upscaling. J Am Ceram Soc 97(2): 543–551.

Mindess S. and Young J. F. (1983) Concrete. Prentice-Hall Inc., Englewood Cliffs, New Jersey, USA.

Mihashi H., Nomura N., Niiseki, S. (1991) Influence of aggregate size on fracture process zone of concrete detected with three dimensional acoustic emission technique. Cement and Concrete Research 21(5): 737-744.

Neville A. M. and Brook J. J. (1990) Concrete Technolog y.Addison Wesley Longman Ltd, Update revision, UK.

536 Rao G.A., Vijayanand I., Eligehausen R. (2010) Studies on ductility and evaluation of
537 minimum flexural reinforcement in RC beams. Materials and Structures 41 (4), 759-
538 771
539 RILEM TC89-FMT (1990) Fracture mechanic of concrete test method. Material and Structures 23:
540 247-252.
541 RILEM TC 50-FCM (1985) Determination of the fracture energy of mortar and concrete by means
542 of three-point bend tests on notched beams. Material and Structures 18(106): 285-290.
543 Shah S. P. and Ahmad S. H. (1994) High performance concrete and its applications. Edward
544 Arnold Press Ltd, UK.
545 Shah S. P., Swartz S. E., Ouyang, C. (1995) Fracture mechanic of concrete. John Willey and sons
546 Inc., Canada, USA.
547 Wolinski S., Hordjik D. A., Reinhardt, H.W. and Cornelissen, H.A.W. (1987) Influence of
548 aggregate size on fracture mechanics parameters of concrete. International journal of cement
549 composites and lightweight concrete 9(3): 95-103.
550 Wu K. R., Chen B., Yao, W., and Zhang, D. (2001). "Effect of coarse aggregate type on
551 mechanical properties of high-performance concrete." Cement and Concrete Research 31(10):
552 1421-1425.
553 Xiao J., Schneider H., Donnecke, C., and Konig, G. (2004) Wedge splitting test on fracture
554 behaviour of ultra high strength concrete. Construction and building materials 18(6): 359-365.
555 Zhang X. and Xu S. (2011) A comparative study of five approaches to evaluate double-K fracture
556 toughness parameters of concrete and size effect analysis. Engineering Fracture Mechanics 78(10):
557 2115-2138.
558 Zhang X. X., Ruiz G., Yu, R.C. and Tarifa, M. (2009) Fracture behaviour of high strength concrete
559 at wide range of loading rates. International Journal of Impact Engineering 36(10-11): 1204-1209.
560 Zhou F. P., Barr B. I. G., and Lydon, F.D. (1995) Fracture properties of high strength concrete
561 with varying silica fume content and aggregates. Cement and Concrete Research 25(3): 543.
562